Soliton absorption spectroscopy

V. L. Kalashnikov* and E. Sorokin†
Institut für Photonik, TU Wien, Gusshausstr. 27/387, A-1040 Vienna, Austria
(Received 18 January 2010; published 23 March 2010)

We analyze optical soliton propagation in the presence of weak absorption lines with much narrower linewidths as compared to the soliton spectrum width by using a perturbation analysis technique based on an integral representation in the spectral domain. The stable soliton acquires a spectral modulation that follows the associated index of refraction of the absorber. The model can be applied to ordinary soliton propagation and to an absorber inside a passively mode-locked laser. In the latter case, a comparison with water vapor absorption in a femtosecond Cr:ZnSe laser yields a very good agreement with experiment. Compared to the conventional absorption measurements in a cell of the same length, the signal is increased by an order of magnitude. The obtained analytical expressions allow further improvement in the sensitivity and spectroscopic accuracy, which makes soliton absorption spectroscopy a promising measurement technique.

DOI: 10.1103/PhysRevA.81.033840 PACS number(s): 42.65.Tg, 42.65.Re, 42.81.Dp, 42.62.Fi

I. INTRODUCTION

Light sources based on femtosecond pulse oscillators have now become widely used tools for studies of ultrafast phenomena, optical metrology, and spectroscopy. Such sources combine broad smooth spectra with diffraction-limited brightness, which is especially important for high-sensitivity spectroscopic applications. Advances in near- and mid-infrared femtosecond oscillators have made it possible to operate in the wavelength ranges of strong molecular absorption, allowing direct measurement of important molecular gases with high resolution and a good signal-to-noise ratio [1]. At the same time, it was observed that such oscillators behave quite differently when the absorbing gas fills the laser cavity or is introduced after the output mirror [2,3]. The issue has become especially important with the introduction of the mid-infrared femtosecond oscillators such as Cr:ZnSe [4], which operate in the 2- to 3-μm wavelength region with strong atmospheric absorption.

As an example, Fig. 1 presents a typical spectrum of a Cr:ZnSe femtosecond oscillator operating under normal atmospheric conditions. It is clear that the pulse spectrum acquires strong modulation features that resemble the dispersion signatures of the atmospheric lines. Being undesirable for some applications, such spectral modulation might at the same time open up interesting opportunities for intracavity absorption spectroscopy. Compared with the traditional intracavity laser absorption spectroscopy [5,6] based on transient processes, this approach would have the advantage of being a well-quantified steady-state technique that can be immediately coupled to frequency combs and optical frequency standards for extreme accuracy and resolution.

In this article, we present a numerical and analytical treatment of the effect of a narrow-band absorption on a femtosecond pulse considered as a dissipative soliton. Such a treatment covers both passively mode-locked ultrashort pulse oscillators with intracavity absorbers and soliton propagation in fibers with impurities. The theoretical results are compared with experiment for a femtosecond Cr:ZnSe oscillator operating under normal atmospheric conditions. We prove that the spectral modulation imposed by a narrow-band absorption indeed accurately follows the associated index of refraction when the absorber linewidth is sufficiently narrow.

II. THE MODEL

Our approach is based on the treatment of an ultrashort pulse as a one-dimensional dissipative soliton of the nonlinear complex Ginzburg-Landau equation (CGLE) [8,9]. This equation has such a wide horizon of application that the concept of "the world of the Ginzburg-Landau equation" has become broadly established [10]. In particular, such a model describes a pulse with the duration T_0 inside an oscillator or propagating along a nonlinear fiber.

To obey the CGLE, the electromagnetic field with the amplitude $A(z,t)$ should satisfy the slowly varying amplitude approximation provided by the relation $\omega_0 \gg 1/T_0$, where ω_0 is the field carrier frequency, t is the local time, and z is the propagation coordinate. This approximation is well satisfied even for pulses of nearly single-optical-cycle duration [11]. When we can additionally neglect the field variation along the cavity round trip or the variation of material parameters along a fiber as well as the contribution of higher-order dispersions, the amplitude dynamics can be described on the basis of the generalized CGLE [9,12–14]:

$$\frac{\partial A(z,t)}{\partial z} = \{-\sigma + \hat{\Sigma}[P(z,t)] - i\gamma P(z,t)\}A(z,t) + \left(\alpha + i\frac{\beta_2}{2}\right)\frac{\partial^2}{\partial t^2}A(z,t) + \hat{\Gamma}[A(z,t)], \quad (1)$$

where $P \equiv |A|^2$ is the instant field power and α is the square of the inverse gain bandwidth. The nonlinear terms in Eq. (1) describe (i) saturable self-amplitude modulation (SAM) with nonlinear gain defined by the nonlinear operator $\hat{\Sigma}$ and (ii) self-phase modulation (SPM) defined by the parameter γ. For a laser oscillator, $\gamma = 4\pi n n_2 l_{\text{cryst}}/(\lambda_0 A_{\text{eff}})$. Here, λ_0 is the wavelength, n and n_2 are the linear and nonlinear refractive indices of an active medium, respectively, l_{cryst} is the length of the active medium, and $A_{\text{eff}} = \pi w^2$ is the effective area of a

*kalashnikov@tuwien.ac.at
†sorokin@tuwien.ac.at

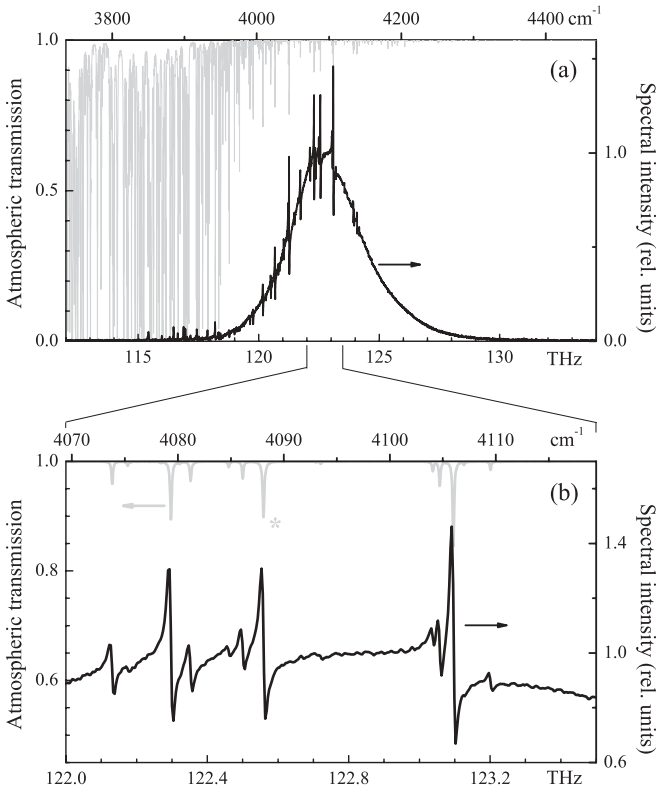

FIG. 1. Output spectrum of a 100-fs Cr:ZnSe oscillator (black solid line) when operated in open air [panel (a)]. The atmospheric transmission (gray) is calculated from the HITRAN database [7] and corresponds to a full round-trip. The lower graph (b) shows the expanded central part of the spectrum. The asterisk denotes the absorption line that is used for quantitative evaluation in the last section.

Gaussian mode with radius w inside the active medium. The propagation coordinate z is naturally normalized to the cavity length (i.e., z becomes the cavity round-trip number). For fiber propagation, $\gamma = 2\pi n n_2/(\lambda_0 A_{\text{eff}})$, where n and n_2 are the linear and nonlinear refractive indices of the fiber, respectively, and A_{eff} is the effective mode area of the fiber [15]. Finally, β_2 is the round-trip net group-delay dispersion (GDD) for an oscillator or the group-velocity dispersion parameter for a fiber with $\beta_2 < 0$, which corresponds to anomalous dispersion.

The typical explicit expressions for $\hat{\Sigma}[P]$ in the case when the SAM response is instantaneous are (i) $\hat{\Sigma}[P] = \kappa P$ (cubic nonlinear gain), (ii) $\hat{\Sigma}[P] = \kappa(P - \zeta P^2)$ (cubic-quintic nonlinear gain), and (iii) $\hat{\Sigma}[P] = \kappa P/(1 + \zeta P)$ (perfectly saturable nonlinear gain) [9,16]. The second case corresponds to a Kerr-lens mode-locked oscillator [8]. The third case represents, for instance, a response of a semiconductor saturable absorber when T_0 exceeds its excitation relaxation time [17]. However, if the latter condition is not satisfied, one has to add an ordinary differential equation to the SAM, and Eq. (1) becomes an integro-differential equation (see below).

The σ term is the saturated net loss at the carrier frequency ω_0, which is the reference frequency in the model. This term is energy dependent: the pulse energy $E(z) \equiv \int_{-\infty}^{\infty} P(z,t)dt$ can be expanded in the vicinity of the threshold value $\sigma = 0$ as $\sigma \approx \delta(E/E^* - 1)$ [18], where $\delta = \ell^2/g_0$ (ℓ is the frequency-independent loss and g_0 is the small-signal gain, both for the round trip) and E^* is the round-trip continuous-wave energy, which is equal to the average power multiplied by the cavity period.

The operator $\hat{\Gamma}$ describes an effect of the frequency-dependent losses, which can be attributed to an absorption within the dissipative soliton spectrum. This effect can be caused, for instance, by the gases filling an oscillator cavity or the fiber impurities for a fiber oscillator. Within the framework of this study, we neglect the effects of loss saturation and let $\hat{\Gamma}$ be linear with respect to $A(z,t)$. The expression for $\hat{\Gamma}[A(z,t)]$ is more convenient to describe in the Fourier domain, with $\tilde{A}(z,\omega)$ being the Fourier image of $A(z,t)$. If the losses result from the l independent homogeneously broadened lines centered at ω_l (relative to ω_0) with linewidths Ω_l and absorption coefficients $\epsilon_l < 0$, then the action of the operator $\hat{\Gamma}$ can be written in the form of a superposition of causal Lorentz profiles [19,20]:

$$\hat{\Gamma}[\tilde{A}] = \left[\sum_l \frac{\epsilon_l}{1 + i(\omega - \omega_l)/\Omega_l}\right]\tilde{A}(z,\omega). \quad (2)$$

In the more general case, the causal Voigt profile has to be used for $\hat{\Gamma}[\tilde{A}]$ [21]. Causality of the complex profile of Eq. (2) demonstrates itself in the time domain, where one has

$$\hat{\Gamma}[A(z,t)] \propto \sum_l \epsilon_l \Omega_l \int_{-\infty}^{t} e^{-(\Omega_l - i\omega_l)(t-t')} A(z,t')\,dt'. \quad (3)$$

The conventional analysis of perturbed soliton propagation includes an approximation of the effective group-delay dispersion of the perturbation as a Taylor series $\beta'(\omega) = \beta_2'(\omega - \omega_0)^2/2 + \beta_3'(\omega - \omega_0)^3/6 + \cdots$, assuming that the additional terms $\beta_2', \beta_3', \ldots$ are sufficiently small. This approach is absolutely not applicable in our case, because the dispersion, associated with a narrow-linewidth absorber can be extremely large. For example, an atmospheric line with a typical width $\Omega = 3$ GHz and a peak absorption of only 10^{-3} produces a group-delay dispersion modulation of $\beta_2' = \pm 0.9$ ns^2, far exceeding the typical intracavity values of $\beta_2 \sim 10^2$ to 10^4 fs^2. Moreover, decreasing the linewidth Ω (and thus reducing the overall absorption of the line) causes the group-delay dispersion term to diverge as $\beta_2' \propto \Omega^{-2}$.

In the following, we shall therefore start with a numerical analysis to establish the applicability and stability of the model, and then present an analysis technique based on an integral representation in the spectral domain.

III. NUMERICAL ANALYSIS

Without introducing any additional assumptions, we solve the Eqs. (1) and (2) numerically by the symmetrized split-step Fourier method. To provide high spectral resolution, the simulation local time window contains 2^{22} points with a mesh interval of 2.5 fs. The simulation parameters for the cubic-quintic version of Eq. (1) are presented in Table I. The GDD parameter $\beta_2 = -1600$ fs^2 provides a stable single pulse with a full width at half maximum of ≈100 fs. The single low-power seeding pulse converges to a steady-state solution over $z \approx 5000$.

The pulse propagation within a linear medium (e.g., an absorbing gas outside an oscillator, a passive fiber containing

TABLE I. Laser simulation parameters. The numbers correspond to the Cr:ZnSe femtosecond oscillator of Fig. 1 with $l_{\text{cryst}} = 0.4$ cm, $w = 80\,\mu$m, $\lambda_0 = 2.5\,\mu$m, $n = 2.44$, $n_2 = 10^{-14}$ cm^2/W, $\ell = 0.075$, and $g_0 = 2.5\ell$.

E^*	γ	α	κ	ζ	δ	β_2
20 nJ	2.5 MW^{-1}	16 fs^2	0.02γ	0.2γ	0.03	-1600 fs^2

some impurities, or a microstructured fiber filled with gas) is described by Eqs. (1) and (2) with zero α, γ, $\hat{\Sigma}$, and the initial $A(0,t)$ corresponding to the output oscillator pulse. The obvious effect of the absorption lines on a pulse spectrum are the dips at ω_l [Fig. 4] that simply follow Beer's law. This regime allows using the ultrashort pulse for conventional absorption spectroscopy [1]. The nonzero real part of an absorber permittivity [i.e., $\text{Im}(\hat{\Gamma}) \neq 0$] significantly changes the pulse in the time domain [22], but does not alter the spectrum. The pulse spectrum reveals only the imaginary part of an absorber permittivity [i.e., $\text{Re}(\hat{\Gamma}) \neq 0$].

Introducing the nonzero SPM coefficient $\gamma = |\beta_2|/(A_0^2 T_0^2)$ with zero α and $\hat{\Sigma}$ transforms Eq. (1) to a perturbed nonlinear Schrödinger equation and results in true perturbed soliton propagation. In this case, as shown in Fig. 2(b), the situation becomes dramatically different. Besides the dips in the spectrum shown by the gray curve corresponding to a contribution of $\text{Re}(\hat{\Gamma})$ only, there is a pronounced contribution from the phase change induced by the dispersion of absorption lines [solid curve in Fig. 2(b) corresponds to the complex profile of $\hat{\Gamma}$ in Eq. (2)]. As a result, the spectral profile has the sharp bends with the maximum on the low-frequency side and the minimum on the high-frequency side of the corresponding absorption line. At the same time, the dips in the spectrum due to absorption are strongly suppressed. In addition to spectral features, the soliton decays, slightly shifts toward the higher frequencies, and its spectrum gets narrower due to the energy loss.

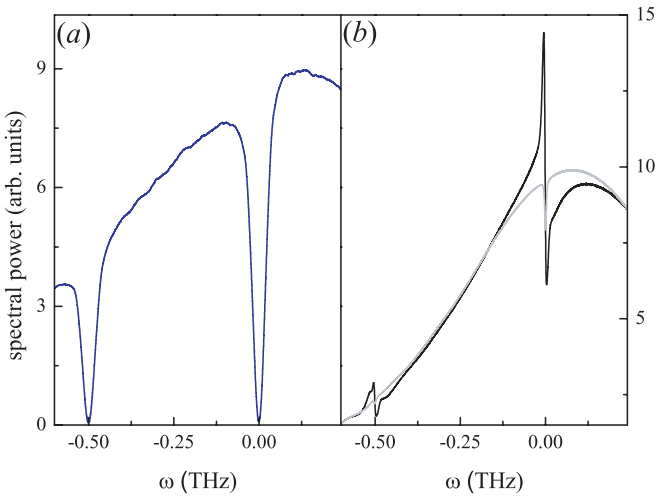

FIG. 2. (Color online) Part of the pulse spectrum after: (a) linear propagation for 25 dispersion lengths inside a fiber with two absorption lines and (b) perturbed soliton propagation for 100 dispersion lengths. The gray curve in (b) corresponds to the contribution of only $\text{Re}(\hat{\Gamma})$ in Eq. (2), the black curve corresponds to the contribution of the complex profile (2). $\epsilon_1 = \epsilon_2 = -0.1$ and $\Omega_1 = \Omega_2 = 40$ GHz. The initial pulse profile is $A(t) = A_0 \text{sech}(t/T_0)$, where $T_0 = 57$ fs.

The soliton spectrum reveals, in this case, the real part of the absorber permittivity. However, the continuous change of the soliton shape due to energy decay renders the problem as a non-steady-state case. The situation becomes different in a laser oscillator, where pumping provides a constant energy flow to compensate the absorption loss.

Let us consider the steady-state intra-cavity narrow-band absorption inside a passively mode-locked femtosecond oscillator, where the pulse is controlled by the SPM and the SAM, which is described by the cubic-quintic $\hat{\Sigma}$ in Eq. (1) modeling the Kerr-lens mode-locking mechanism [12]. Such an oscillator can operate both in the negative dispersion regime [12] with a chirp-free soliton-like pulse and in the positive dispersion regime [18] where the propagating pulse acquires a strong positive chirp. In this study, we consider only the negative dispersion regime; the positive dispersion regime will be a subject of following studies.

The results of the simulation are shown in Figs. 3 and 4, and they demonstrate the same dispersion-like modulation of the pulse spectrum. Figure 3 demonstrates action by three narrow ($\Omega = 2$ GHz) absorption lines centered at -10, 0 and 10 GHz in the neighborhood of $\omega = 0$. One can see [Fig. 3(a)] that the absorption lines do not cause spectral dips at ω_l, but produce sharp bends, very much like the case of the true perturbed Schrödinger soliton considered before. One can also clearly see the collective redistribution of spectral power from higher to lower frequencies, which enhances local spectral asymmetry [Fig. 3(a)]. Such an asymmetry suggests that the dominating contribution to a soliton perturbation results from the real part of an absorber permittivity, which, in particular, causes the time asymmetry of the perturbation in the time domain. This asymmetry is seen in the time domain as a ns-long modulated exponential precursor in Fig. 3(b).

The simulated effect of a single narrow absorption line centered at $\omega = 0$ is shown in Fig. 4 for different values

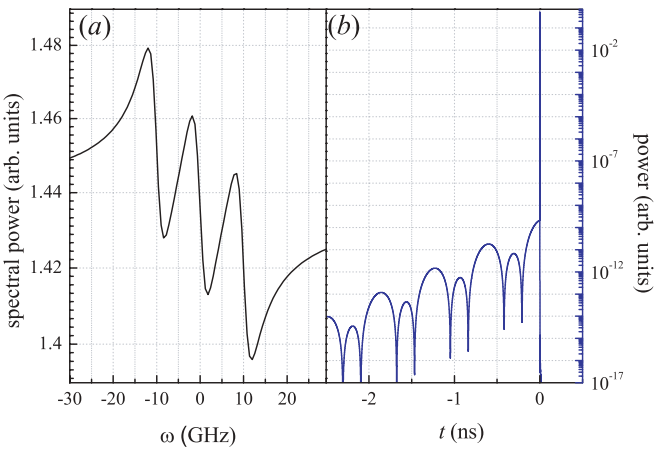

FIG. 3. (Color online) Dissipative soliton in an oscillator: (a) central part of the spectrum and (b) power $P(t)$. An oscillator is filled with an absorber described by Eq. (2) with a triplet of lines: $\epsilon_1 = \epsilon_2 = \epsilon_3 = -0.005$, $\Omega_1 = \Omega_2 = \Omega_3 = 2$ GHz, and $\omega_1 = -10$, $\omega_2 = 0$, $\omega_3 = 10$ GHz.

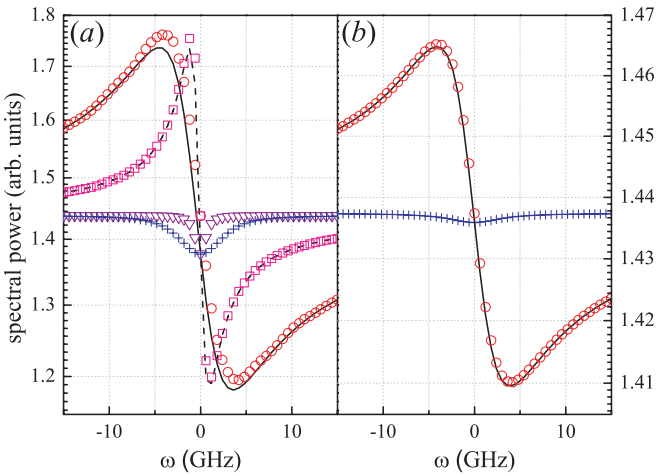

FIG. 4. (Color online) Central parts of the dissipative soliton spectra in an oscillator with the single absorption line centered at $\omega = 0$. (a) $\epsilon = -0.05$, $\Omega = 4$ GHz (solid curve, open circles, and crosses) and 1 GHz (dashed curve, open squares, and triangles). (b) $\epsilon = -0.005$ and $\Omega = 4$ GHz. The solid and dashed curves correspond to the contribution of $\hat{\Gamma}$ described by Eq. (2). Open circles and squares describe the separate contribution of $\mathrm{Im}(\hat{\Gamma})$. Crosses and triangles describe the separate contribution of $\mathrm{Re}(\hat{\Gamma})$.

of peak absorption ϵ and width Ω. In Fig. 4(a), $\epsilon = -0.05$ and $\Omega = 4$ GHz (solid curve, open circles, and crosses) and 1 GHz (dashed curve, open squares, and open triangles). The solid and dashed curves demonstrate the action of the complex profile (2), whereas the circles (squares) and crosses (triangles) demonstrate the separate action of $\mathrm{Im}(\hat{\Gamma})$ and $\mathrm{Re}(\hat{\Gamma})$, respectively. One can see that the profile of the perturbed spectrum traces that formed by only $\mathrm{Im}(\hat{\Gamma})$ (i.e., the perturbed spectrum traces the real part of the absorber permittivity). One can say that the pure-phase effect [$\mathrm{Im}(\hat{\Gamma})$, circles and squares in Figs. 4(a) and 4(b)] strongly dominates pure absorption [$\mathrm{Re}(\hat{\Gamma})$, crosses in Figs. 4(a) and 4(b)], like that for the Schrödinger soliton. Such a domination is enhanced with a lowered ϵ [Fig. 4(b), crosses]; however, the $|\epsilon|$ growth increases the relative contribution of $\mathrm{Re}(\hat{\Gamma})$ and causes the frequency downshift of the bend [Fig. 4(a)]. The amplitude of the bend traces ϵ, while its width is defined by Ω.

The SAM considered above is modeled by the cubic-quintic nonlinear term $\hat{\Sigma}$ in Eq. (1). Such a SAM is typically realized by using the self focusing inside an active medium (Kerr-lens mode locking). For reliable self-starting operation of a mode-locked oscillator it is often desirable to use a suitable saturable absorber (SA), such as a semiconductor saturable mirror [23,24]. Such an absorber can be described in the simplest case by a single-lifetime two-level model, giving the time-dependent loss coefficient $\Lambda(t)$ as

$$\frac{\partial \Lambda(t)}{\partial t} = \frac{\Lambda_0 - \Lambda(t)}{T_s} - \Lambda(t)\frac{P(t)}{J_s A_{\mathrm{eff}}}, \tag{4}$$

where Λ_0 is the loss coefficient for a small signal, A_{eff} is the effective beam area on the SA, and T_s and J_s are the SA relaxation time and the saturation energy fluency, respectively. Equation (4) supplements Eq. (1), and the SAM term $\hat{\Sigma}$ in the latter has to be replaced by $[\Lambda_0 - \Lambda(t)]$. When the pulse width is longer than the SA relaxation time, one can replace Eq. (4) by its adiabatic solution so that

$$\hat{\Sigma} = \frac{\eta_0 \xi P(t)}{1 + \xi P(t)}, \tag{5}$$

where $\xi \equiv T_s/(J_s A_{\mathrm{eff}})$ is the inverse saturation power.

We have simulated Eqs. (1), (2), and (4) in the case of $J_s = 50\ \mu\mathrm{J/cm}^2$ and $T_s = 0.5$ ps, which corresponds to the measurement in Fig. 1. Two cases have been considered: weak focusing ($A_{\mathrm{eff}} = 4000\ \mu\mathrm{m}^2$ or saturation energy $E_s = 2$ nJ) and hard focusing ($A_{\mathrm{eff}} = 1000\ \mu\mathrm{m}^2$ or saturation energy $E_s = 0.5$ nJ). We also considered Eq. (5) for the same peak saturation level as weakly focused SA (i.e., $\xi^{-1} = 4$ kW). In the latter case, the SA effectively becomes instantaneous, and the perturbed soliton spectrum is the same as for Kerr-lens mode locking (i.e., same as for the cubic-quintic $\hat{\Sigma}$). When the saturation energy is sufficiently large, there is no difference between the models expressed by Eqs. (4) and (5). The effect of a narrow absorption line is similar to that of the soliton of the cubic-quintic Eq. (1). A decrease of the saturation energy E_s causes a downshift of the pulse spectrum as a whole, but the narrow bend on the soliton spectrum reproduces the real part of the absorber permittivity. One can thus conclude that the type of the SAM is irrelevant for an effect of the narrow-band absorption lines on a dissipative soliton spectrum.

Another important conclusion from the numerical simulations is the demonstrated stability of the dissipative soliton against perturbations induced by narrow-band absorption. In the following analytical treatment we shall therefore omit the stability analysis.

IV. PERTURBATIVE ANALYSIS OF SOLITON SPECTRUM

To study the transformation of the dissipative soliton spectrum under the action of narrow absorption lines, we apply the perturbation method [9,25]. Because the basic features already become apparent for the perturbed Schrödinger soliton and do not depend on SAM details, we shall consider the simplest case of the cubic nonlinear gain $\hat{\Sigma}[P] = \kappa P$. The unperturbed solitonic chirp-free solution of such a reduced equation with $\hat{\Gamma} = 0$ is $a(z,t) = A_0 \mathrm{sech}(t/T_0)\exp[i\phi(t) + iqz]$ with $d\phi/dt = \varpi$. The unperturbed soliton parameters are [25]

$$\begin{aligned} \varpi &= 0, \\ A_0^2 &= \frac{2\alpha}{\kappa T_0^2}, \\ q &= \frac{\beta_2}{2T_0^2}, \\ T_0 &= \sqrt{\frac{\alpha}{\sigma}}, \end{aligned} \tag{6}$$

where the equation parameters are confined

$$\begin{aligned} \beta_2 &= -2\frac{\alpha\gamma}{\kappa}, \\ \sigma &> 0. \end{aligned} \tag{7}$$

Thus, the soliton wave number is $q = -\gamma\sigma/\kappa$.

Its is reasonable to treat the soliton of the reduced Eq. (1) as the Schrödinger soliton with the parameters constrained by the dissipative terms σ, α, and κ [see Eqs. (6) and (7)]. This implies

that the equation, which has to be linearized with respect to a small perturbation copropagating with the soliton without beating, decay, or growth (i.e., having a real wave number that equals q [9]), is the perturbed nonlinear Schrödinger equation:

$$\frac{\partial A(z,t)}{\partial z} = i\frac{\beta_2}{2}\frac{\partial^2}{\partial t^2}A(z,t) - i\gamma P(z,t)A(z,t) + \hat{\Gamma}[A(z,t)]. \tag{8}$$

Linearization of the latter with respect to a perturbation $f(t)\exp(iqz)$ results in

$$iqf(t) = i\frac{\beta_2}{2}\frac{d^2 f(t)}{dt^2} - i\gamma[2|a(t)|^2 f(t) + a(t)^2 f^*(t)] + \hat{\Gamma}(a+f). \tag{9}$$

In the spectral domain, Eq. (9) becomes

$$[k(\omega)-q]\tilde{f}(\omega) + \frac{1}{\pi}\int_{-\infty}^{\infty} d\omega' U(\omega-\omega')\tilde{f}(\omega') + \frac{1}{2\pi}\int_{-\infty}^{\infty} d\omega' U(\omega-\omega')\tilde{f}^*(\omega') = S(\omega), \tag{10}$$

where [25]

$$U(\omega) = -\pi\gamma T_0^2 A_0^2 \omega \operatorname{csch}(\pi T_0\omega/2),$$
$$S(\omega) = \frac{iA_0\pi T_0}{\cosh(\pi T_0\omega/2)}\sum_l \epsilon_l \frac{1 - i(\omega-\omega_l)/\Omega_l}{1+(\omega-\omega_l)^2/\Omega^2}, \tag{11}$$
$$k(\omega) = -\frac{\beta_2}{2}\omega^2 - \sum_l \epsilon_l \frac{(\omega-\omega_l)/\Omega_l + i}{1+(\omega-\omega_l)^2/\Omega^2}.$$

Here, $k(\omega)$ is the frequency-dependent complex wave number and $S(\omega)$ is the perturbation source term for $\hat{\Gamma}$ corresponding to Eq. (2).

Furthermore, one may assume phase matching between the soliton and its perturbation. This assumption, in combination with the equality $U(\omega) = U^*(\omega)$ that holds for the Schrödinger soliton, results in $\int_{-\infty}^{\infty} d\omega' U(\omega-\omega')\tilde{f}^*(\omega') = \int_{-\infty}^{\infty} d\omega' U(\omega-\omega')\tilde{f}(\omega')$.

Equation (10) for the Fourier image of the perturbation is the Fredholm equation of the second kind. Its solution can be obtained by the Neumann series method so that the iterative solution becomes [25]

$$\tilde{f}_n(\omega) = \frac{S(\omega)}{k(\omega)-q} - \frac{3}{2\pi[k(\omega)-q]} \times \int_{-\infty}^{\infty} d\omega' U(\omega-\omega')\tilde{f}_{n-1}(\omega'), \tag{12}$$

where $\tilde{f}_n(\omega)$ is the n-th iteration and $\tilde{f}_0(\omega) = S(\omega)/[k(\omega)-q]$.

The "phase character" of a soliton perturbation [i-multiplier in left-hand side of Eq. (9) and the expression for the source term (11)] demonstrates that the real part of the absorber permittivity contributes to the real part of the soliton spectral amplitude. Simultaneously, the resonant condition $k(\omega) - q = 0$, which is responsible for a dispersive wave generation caused by, for instance, the higher-order dispersions [9], is not reachable in our case. The resonance can appear in cases of large $|\epsilon|$, κ/γ, and $\Omega_l T_0$, but such regimes are beyond the scope of this work.

Equation (12) can be solved numerically. Figure 5 shows $\mathrm{Re}[\tilde{f}_1(\omega)]$ (dashed curve) and $\mathrm{Im}[\tilde{f}_1(\omega)]$ (dotted curve). One can see that the real part of the absorber permittivity defines $\mathrm{Re}[\tilde{f}(\omega)]$, while the imaginary part of the absorber permittivity defines $\mathrm{Im}[\tilde{f}(\omega)]$. This agrees with the simulation results and is contrary to the case of linear pulse propagation. One can also see a tiny frequency downshift θ of the $\tilde{f}(\omega)$ minimum from ω_l like that in the simulations.

The pulse spectrum (solid curve in Fig. 5), results from interference of the perturbation with the soliton. For the chosen parameters of the absorption line, the zero-order approximation $\tilde{f}_0(\omega)$ (open squares) is very close to the first-order approximation (solid curve) but is slightly downshifted in the vicinity of the bend maximum and minimum.

With an even narrower linewidth Ω of 1 GHz (Fig. 6), the spectral perturbation gets very close to the real part of absorber permittivity and, simultaneously, the spectral downshift θ [location of the $\mathrm{Im}(\tilde{f}_1)$ minimum, dashed curve] vanishes. The curve $\tilde{f}_0(\omega)$ (gray solid curves) now perfectly matches the curve $\tilde{f}_1(\omega)$ (open circles and crosses) within a broad range of ϵ (gray solid curves 1 and 2 as well as circles and crosses belong to $\epsilon = -0.005$ and -0.05, respectively). The bend amplitudes are in agreement with Eq. (11).

A superposition of three identical absorption lines, which corresponds to the numerical spectra in Fig. 2, is shown in Fig. 7. One can see that the lowest-order analytical solution $\tilde{f}_0(\omega)$ accurately reproduces the numerical result. It is important that a cumulative contribution of lines into $k(\omega)$ does not distort a superposition contribution of $S(\omega)$ into a soliton spectrum [see Eqs. (11) and (12)]. This means that the individual contribution of a single line within a group is easily distinguishable and can be quantitatively assessed, opening the way for interesting spectroscopic applications.

As Figs. 5 and 6 suggest, the zero-order approximation $\tilde{f}_0(\omega) = S(\omega)/[k(\omega)-q]$ is quite accurate for a description of the perturbation in the limit of $|\epsilon| \ll 1$. This makes it possible to express the perturbed spectrum of an isolated line [see Eqs. (11) and (12)] in analytical form [25]:

$$\tilde{P}(\omega) \equiv |\tilde{a}(\omega) + \tilde{f}_0(\omega)|^2 \approx \frac{A_0^2\pi^2 T_0^2 \operatorname{sech}\left(\frac{\pi T_0\omega}{2}\right)^2 \left(\frac{\beta_2}{2}\omega^2 + q\right)^2 \left[1 + \frac{(\omega-\omega_l)^2}{\Omega_l^2}\right]}{\epsilon_l^2 + \frac{2(\omega-\omega_l)\epsilon_l}{\Omega_l}\left(\frac{\beta_2}{2}\omega^2 + q\right) + \left(\frac{\beta_2}{2}\omega^2 + q\right)^2 \left[1 + \frac{(\omega-\omega_l)^2}{\Omega_l^2}\right]}. \tag{13}$$

Equation (13) allows further simplification in the case of $|\epsilon| \ll 1$:

$$\tilde{P}(\omega) \approx A_0^2\pi^2 \operatorname{sech}\left(\sqrt{\frac{\alpha}{\sigma}}\frac{\pi\omega}{2}\right)^2 \frac{\alpha}{\sigma}\left\{1 + \frac{2\epsilon_l\kappa}{\gamma\left(\alpha\omega_l^2 + \sigma\right)}\frac{(\omega-\omega_l)}{\left[1 + \frac{(\omega-\omega_l)^2}{\Omega_l^2}\right]\Omega_l}\right\}, \tag{14}$$

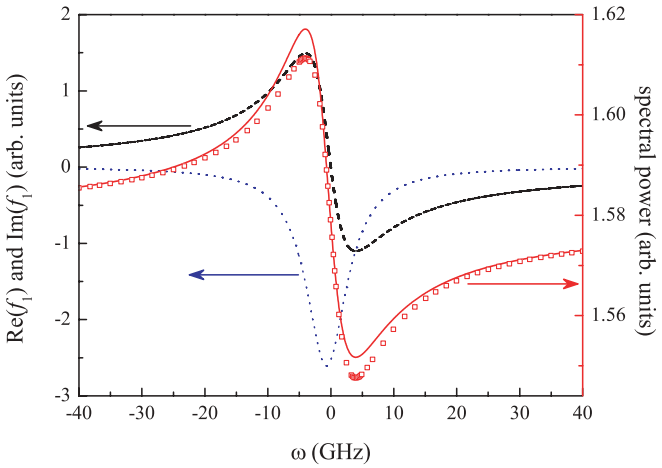

FIG. 5. (Color online) Central part of the dissipative soliton spectra perturbed by $\tilde{f}_1(\omega)$ (solid curve) or $\tilde{f}_0(\omega)$ (open squares) as well as the profiles of Re($\tilde{f}_1$) (dashed curve) and Im($\tilde{f}_1$) (dotted curve) from Eq. (12). The single absorption line is centered at ω =0, $\epsilon = -0.005$, and $\Omega = 4$ GHz.

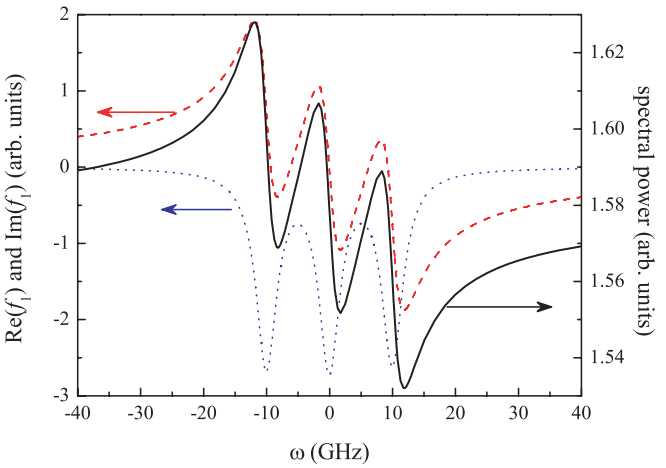

FIG. 7. (Color online) Central part of the dissipative soliton spectra perturbed by $\tilde{f}_0(\omega)$ (black solid curve) and profiles of Re($\tilde{f}_0$) (dashed curve) and Im($\tilde{f}_0$) (dotted curve) from Eq. (12). The triplet of absorption lines is centered at $\omega_1 = -10$, ω_2 =0, $\omega_3 = 10$ GHz, $\epsilon_1 = \epsilon_2 = \epsilon_3 = -0.005$, and $\Omega_1 = \Omega_2 = \Omega_3 = 2$ GHz.

where Eqs. (6) and the condition $\alpha\Omega_l^2 \ll 1$ have been used.

Equation (14) demonstrates that the spectral bend follows the real part of the absorber permittivity. The spectral downshift of the bend is an effect of $O(\epsilon^2)$ and is not included in Eq. (14). The perturbation is represented by the term in square brackets and its relative amplitude is proportional to ϵ. Furthermore, the aspect ratio of the kink grows with (i) the increase of the relative contribution of the SAM κ/γ, (ii) the gain bandwidth $1/\sqrt{\alpha}$, (iii) the approach of the resonance frequency ω_l to the center of soliton spectrum [but the ratio of the aspect ratio to the local soliton spectral power increases with $|\omega_l|$ because the former decreases as ω_l^{-2} whereas the latter falls faster as $\cosh(\pi T_0\omega_l/2)^2$], and (iv) the approach to the soliton stability border, which corresponds to vanishing σ. It should be noted that smaller σ entails growth in the soliton width [Eq. (6)].

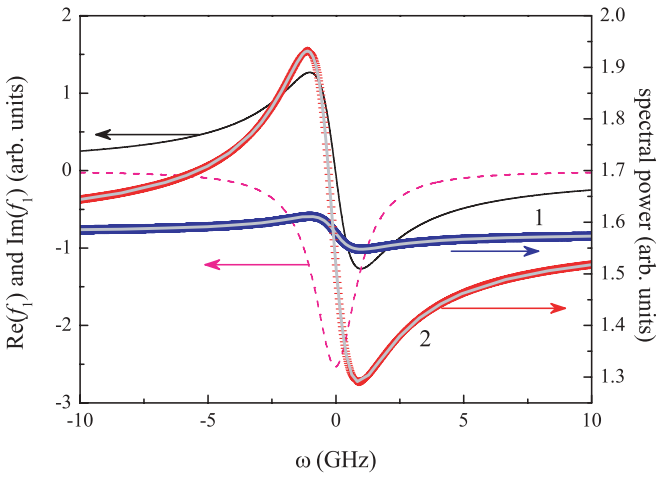

FIG. 6. (Color online) Central part of the dissipative soliton spectra perturbed by $\tilde{f}_1(\omega)$ (open circles and crosses) or $\tilde{f}_0(\omega)$ (solid gray curves) as well as the profiles of Re($\tilde{f}_1$) (solid black curve) and Im($\tilde{f}_1$) (dashed curve) from Eq. (12). The single absorption line with $\Omega = 1$ GHz is centered at $\omega = 0$, $\epsilon = -0.005$ (black solid and dashed curves as well as open circles and solid gray curve 1), and $\epsilon = -0.05$ (crosses and solid gray curve 2).

Because the soliton parameters are interrelated, it is instructive to express σ through the observable parameters such as the soliton energy E or the soliton width T_0. When $\alpha\omega_l^2 \ll \sigma$ (e.g., $\omega_l \approx 0$ or an oscillator operating far from the stability border σ =0), the perturbation amplitude is inversely proportional to $\gamma\kappa E^2$:

$$\frac{2\epsilon_l\kappa}{\gamma\left(\alpha\omega_l^2+\sigma\right)} \approx \frac{32\epsilon_l\alpha}{\gamma\kappa E^2} = \frac{2\epsilon_l\kappa T_0^2}{\gamma\alpha}. \tag{15}$$

For a fixed gain bandwidth, the amplitude scales with the pulsewidth squared: T_0^2. Ultimately, the latter equation is equivalent to

$$\frac{2\epsilon_l\kappa}{\gamma\left(\alpha\omega_l^2+\sigma\right)} \approx -\frac{2\epsilon_l}{q}. \tag{16}$$

That is, the relative perturbation amplitude near the soliton central frequency is the ratio of the incurred loss coefficient to the soliton wave number, regardless of the z-coordinate normalization. Therefore, this analytical expression that has been derived for the self-consistent oscillator should also be valid for soliton propagation in a long fiber when the conditions of applicability $|\epsilon| \ll 1$ and $\Omega_l \ll 1/T_0$ are met. The final form of the soliton spectrum thus becomes

$$\tilde{P}(\omega) = \tilde{P}_0(\omega)\left[1 - \frac{2}{q}\sum_l \epsilon_l \frac{(\omega-\omega_l)/\Omega_l}{1+\frac{(\omega-\omega_l)^2}{\Omega_l^2}}\right], \tag{17}$$

where $\tilde{P}_0(\omega)$ is the spectrum of an unperturbed soliton.

V. DISCUSSION

In the analysis above we have shown that, for the case of sufficiently sparse, narrow, and weak Lorentzian absorber lines, their spectral signatures are equivalent to the dispersion-like modulation with a relative amplitude equal to the peak

absorption coefficient over the oscillator round trip (or nonlinear length for passive propagation) divided by the soliton wave number. For quantitative comparison with the experiment we recall Eq. (6) and express the maximum spectrum deviation of a single line at $|\omega - \omega_l| = \Omega_l$ through observable parameters:

$$\left|\frac{\epsilon_l}{q}\right| = \chi_l L \frac{T_0^2}{|\beta_2|} = \chi_l L \frac{0.0319}{|\beta_2|(\Delta\nu)^2}, \tag{18}$$

where $\chi_l = 2\epsilon_l$ is the peak absorption coefficient of the line, L is the absorber path length, and $\Delta\nu$ is the full width at half maximum of the soliton spectrum. Substituting the actual values of the setup in Fig. 1 ($\beta_2 = -820 \pm 40$ fs^2, $\Delta\nu = 113\,\mathrm{cm}^{-1} = 3.39$ THz, round-trip air-path length $L = 149$ cm, relative humidity $50\% \pm 1\%$ at $21 \pm 0.5^\circ$C) and taking, for example, the line at 4088 cm^{-1} (122.56 THz, marked with an asterisk), we obtain $|\epsilon/q| = 0.33 \pm 0.02$ for the maximum modulation, which is in perfect agreement with the observed value of 31.5% [Fig. 1(b), black line]. The agreement is remarkably accurate given the less-than-optimal resolution of the spectrometer (0.25 cm^{-1}) and significant third-order dispersion of about $+10^4$ fs^3 that was not accounted for in the present analysis.

It is important to notice that the expression (18) includes only the externally observable soliton bandwidth and the relatively stable dispersion parameter. The alignment-sensitive values like the saturated losses σ, nonlinearity γ, nonlinearity saturation parameter κ, etc., which are in practice not known with sufficient accuracy, are all accounted for by the self-consistent soliton parameters.

Another important point is the fact that the signal amplitude $2|\epsilon/q|$ can be much bigger than that from conventional absorption spectroscopy $\chi_l L$ from a cell with the same length. The signal-enhancement factor can be controlled by the pulse parameters and it exceeds an order of magnitude for the present case ($\chi_l L = 5\%$ for the selected line and a single-pass cell of resonator size). For additional sensitivity improvement one can apply the well-developed intracavity multipass cell technique [26]. The expression (18) suggests that ultimate sensitivity can be obtained at the expense of the reduced bandwidth coverage $\Delta\nu$. In this respect, the present technique has the same quadratic dependence of sensitivity on spectral bandwidth as conventional intracavity absorption spectroscopy [5].

Further refinement of the present theory should include a demonstration of its applicability to arbitrarily shaped absorption features. The superposition property provides a strong argument for such an extension, but it has to be rigorously proven for Doppler- and more general Voigt-shaped lines and also for the dense line groups in, for example, Q branches. It would be interesting also to extend the theory to the absorber lines at the soliton wings [Fig. 1(a)].

With the above issues resolved, the soliton-based spectroscopy may become a powerful tool for high-resolution, high-sensitivity spectroscopy and sensing. Possible implementations include soliton propagation in gas-filled holey fibers, as well as already presented intracavity spectroscopy with femtosecond oscillators. The latter, being a natural frequency-comb source, allows direct locking to optical frequency standards, providing for ultimate resolution and spectral accuracy.

VI. CONCLUSION

We have been able to derive an analytical solution to the problem of a one-dimensional optical dissipative soliton propagating in a medium with narrow-band absorption lines. We predict the appearance of spectral modulation that follows the associated index of refraction rather than the absorption profile. The perturbation analysis technique is based on integral representation in the spectral domain and is insensitive to the diverging differential terms inherent to the Taylor series representation of the narrow spectral lines.

The model is applicable to a conventional soliton propagation and to a passively mode-locked laser with intracavity absorber; the only difference being the characteristic propagation distance (dispersion length and cavity round trip, respectively). In the latter case the prediction has been confirmed for a case of water vapor absorption lines in a mid-IR Cr:ZnSe oscillator. The model provides very good qualitative and quantitative agreement with experimental observations, opening a way to metrology and spectroscopic applications of the technique, which can provide a significant (order of magnitude and more) enhancement of the signal over conventional absorption for the same cell length.

ACKNOWLEDGMENTS

We gratefully acknowledge insightful discussions and experimental advice from N. Picqué, G. Guelachvili (CNRS, Univ. Paris-Sud, France), and I. T. Sorokina (NTNU, Norway). This work has been supported by the Austrian Science Fund FWF (projects 17973 and 20293) and the Austrian-French Collaboration Amadée.

[1] E. Sorokin, I. T. Sorokina, J. Mandon, G. Guelachvili, and N. Picqué, Opt. Express **15**, 16540 (2007).

[2] J. Mandon, G. Guelachvili, I. Sorokina, E. Sorokin, V. Kalashnikov, and N. Picqué, *Europhysics Conference Abstract 32G* (European Physical Society, Paris, 2008), paper WEoB.4 at Europhoton 2008.

[3] V. Kalashnikov, E. Sorokin, J. Mandon, G. Guelachvili, N. Picqué, and I. T. Sorokina, *Europhysics Conference Abstract 32G* (European Physical Society, Paris, 2008), paper TUoA.3 at Europhoton 2008.

[4] I. T. Sorokina, E. Sorokin, and T. Carrig, in *Conference on Lasers and Electro-Optics/Quantum Electronics and Laser Science Conference and Photonic Applications Systems Technologies, Technical Digest (CD)* (Optical Society of America, 2006), paper CMQ2.

[5] V. M. Baev, T. Latz, and P. E. Toschek, Appl. Phys. B **69**, 171 (1999).

[6] N. Picqué, F. Gueye, G. Guelachvili, E. Sorokin, and I. T. Sorokina, Opt. Lett. **30**, 3410 (2005).

[7] The HITRAN database http://www.cfa.harvard.edu/hitran/.

[8] H. A. Haus, J. G. Fujimoto, and E. P. Ippen, J. Opt. Soc. Am. B **8**, 2068 (1991).
[9] N. N. Akhmediev and A. Ankiewicz, *Solitons: Nonlinear Pulses and Beams* (Chapman&Hall, London, 1997).
[10] I. S. Aranson and L. Kramer, Rev. Mod. Phys. **74**, 99 (2002).
[11] T. Brabec and F. Krausz, Phys. Rev. Lett. **78**, 3282 (1997).
[12] *Few-Cycle Laser Pulse Generation and its Applications*, edited by F. X. Kärtner (Springer Verlag, Berlin, 2004).
[13] *Dissipative Solitons*, edited by N. N. Akhmediev and A. Ankiewicz (Springer Verlag, Berlin, 2005).
[14] The signs before i in Eq. (1) correspond to those in [8] and S. A. Akhmanov, V. A. Vysloukh, and A. S. Chirkin, *Optics of Femtosecond Laser Pulses* (AIP, NY, 1992).
[15] G. P. Agrawal, *Nonlinear Fiber Optics* (Academic Press, San Diego, 2001).
[16] A. Biswas and S. Konar, *Introduction to Non-Kerr Law Optical Solitons* (Chapman&Hall, Boca Raton, 2007).
[17] H. A. Haus, Y. Silberberg, J. Opt. Soc. Am. B **2**, 1237 (1985).
[18] V. L. Kalashnikov, E. Podivilov, A. Chernykh, and A. Apolonski, Appl. Phys. B **83**, 503 (2006).
[19] V. S. Butylkin, A. E. Kaplan, Yu. G. Khronopulo, and E. I. Yakubovich, *Resonant Nonlinear Interactions of Light with Matter* (Springer Verlag, Berlin, 1989).
[20] K. E. Oughstun, *Electromagmetic and Optical Pulse Propagation 1* (Springer, New York, 2006).
[21] D. De Sousa Meneses, G. Gruener, M. Malki, and P. Echegut, J. Non-Cryst. Solids **351**, 124 (2005).
[22] Y. Yamaoka, L. Zeng, K. Minoshima, and H. Matsumoto, Appl. Opt. **43**, 5523 (2004).
[23] M. N. Islam, E. R. Sunderman, C. E. Soccolich, I. Bar-Joseph, N. Sauer, T. Y. Chang, and B. I. Miller, IEEE J. Quantum Electron. **25**, 2454 (1989).
[24] U. Keller, K. J. Weingarten, F. X. Kärtner, D. Kopf, B. Braun, I. D. Jung, R. Fluck, C. Honninger, N. Matuschek, and J. Aus der Au, IEEE J. Sel. Top. Quantum Electron. **2**, 435 (1996).
[25] V. L. Kalashnikov, Maple worksheet (unpublished) http://info.tuwien.ac.at/kalashnikov/perturb1.html.
[26] A. M. Kowalevicz, A. Sennaroglu, A. T. Zare, and J. G. Fujimoto, J. Opt. Soc. Am. B **23**, 760 (2006).